J Appl Electrochem (2009) 39:545–551
DOI 10.1007/s10800-008-9743-8

ORIGINAL PAPER

Interconnect materials for next-generation solid oxide fuel cells

Paolo Piccardo · Roberta Amendola · Sébastien Fontana · Sébastien Chevalier · Gilles Caboches · Paul Gannon

Received: 3 September 2008 / Accepted: 1 December 2008 / Published online: 6 January 2009

Abstract Highly-efficient solid oxide fuel cell (SOFC) systems are gaining increased attention for future energy conversion applications. Many planar SOFC stack designs utilise ferritic stainless steel (FSS) interconnect components. During operation, surface corrosion of FSS interconnects degrades stack operation by increasing electrical resistance and introducing other deleterious material interactions. To minimise these effects, various surface modifications and coatings are currently under investigation. Two of these methods under development for this application are: metal organic chemical vapour deposition (MO-CVD); and, large area filtered arc deposition (LAFAD). SOFC interconnect-relevant corrosion behaviour of an MO-CVD coating on Crofer 22 APU, AL453, Fe30Cr and Haynes230, and complex, amorphous LAFAD AlCrCoMnTiYO coatings on FSS 430 were investigated. Both of these surface modifications and coatings exhibit significantly improved corrosion protection as compared with uncoated FSS samples.

P. Piccardo (✉) · R. Amendola
Department of Chemistry and Industrial Chemistry (DCCI), Università di Genova, Genoa, Italy
e-mail: pol@chimica.unige.it

P. Piccardo · R. Amendola
CNR – IENI, Genoa Research Unit, Genoa, Italy

S. Fontana · S. Chevalier · G. Caboches
Institut Carnot de Bourgogne, UMR 5209 CNRS, Université de Bourgogne, Dijon, France

P. Gannon
Department of Chemical and Biological Engineering, Montana State University, Bozeman, MT, USA

Keywords SOFC · Metallic interconnects · High-temperature oxidation · Thermal barrier coatings · MOCVD

1 Introduction

One of the most challenging issues facing Solid Oxide Fuel Cell (SOFC) system development is cost [1, 2]. High-temperature SOFCs (~1000 °C) require expensive ceramic materials, which can tolerate extreme operating conditions. Cell interconnection, especially with planar designs, has historically met with difficulty, and often dominates cell and stack degradation processes. Ceramic interconnects, e.g. Ca-doped $LaCrO_3$, were used widely for high-temperature SOFCs; however, difficulties in fabrication and high cost were limiting. The tubular SOFC stack design by Siemens Westinghouse is considered one of the best products [3] and is favoured for its efficiency, stability and seal-less design.

Advances in SOFC component development has effectively lowered operating temperatures, e.g., to about 800 °C), which enables a wider-selection of interconnection materials, including metals and metal alloys. As SOFC operating temperatures continue to decrease (e.g. to about 700 °C, selection of interconnect materials able to remain stable during simultaneous exposure to both highly oxidising and wet reducing atmospheres for >40,000 h becomes easier.

Metals in general are highly sensitive to oxygen at high temperatures and can change physical properties when hydrogen diffuses into the alloy. The interaction with the other SOFC components is another fundamental aspect, and to summarise the functional criteria of SOFC interconnects, they must: provide low resistance contact to adjoining electrodes, exhibit chemical and physical compatibility and stability with adjoining electrodes and seals,

and be inexpensive, in respect of both materials and fabrication. At an SOFC operating temperature of 800 °C, several candidate metal alloys have been investigated, including: Nickel-based, Chromium-based and Iron-based alloys. In every case, some of the performance criteria were met; however, others remained out of reach, thus prohibiting these un-modified materials as SOFC interconnects.

Of the materials examined to-date, ferritic stainless steel (FSS) appears to be the best option for SOFC interconnects (ICs). This is due to several features: coefficients of thermal expansion compatible with other cell components, relatively low area-specific resistance, especially short-term, ease in formability and low cost. Therefore FSS is often used as interconnects in planar SOFC stacks, which separate fuel and oxidant gasses and connect individual cells into electrical series in a physical cell stack. During operation, a chromia (Cr_2O_3)-based thermally-grown oxide (TGO) layer forms and grows on FSS surfaces at the IC/cathode (air electrode) interface. The TGO layer growth and structural evolution depends on FSS alloy characteristics, such as composition and microstructure, and exposure conditions, e.g., oxidising gas composition and contacting solids. Complex, stratified TGO layers often evolve on FSS surfaces during SOFC cathode gas phase exposures, forming several different condensed phases e.g. Cr_2O_3, $(Cr,Mn)_3O_4$, SiO_2 and/or Fe_2O_3. After SOFC-IC exposure over thousands of hours, the TGO layer on FSS often grows to >10 μm, dominated by a Cr_2O_3 base layer, and can exhibit localised exfoliation due to energy release from residual stresses built up within the TGO layer. Continued TGO layer growth and formation of insulating oxides (e.g., SiO_2) also introduces increased contact resistance with adjoining electrodes, measured as area specific resistance, or ASR. In addition, Cr-transport from TGO layers in either or both solid and gas phases into cathodes and cathode/electrolyte interfaces has been indicted in SOFC stack performance degradation. Moreover, simultaneous "dual atmosphere" exposure, e.g., fuel at anode side and air at cathode side, can induce anomalous and/or accelerated corrosion on the SOFC-IC air (cathode) side. In this context, anomalous oxidation during dual atmosphere exposures is described as the development of a TGO layer with significantly different composition and microstructure compared with the single atmosphere counterpart. Dual atmosphere exposure can also result in a substantial increase in total air-side TGO layer thickness formed vs. single atmosphere exposure.

Standard and modified FSS compositions, e.g., 430, 439, 441, 453 and Crofer 22APU are being investigated for the SOFC-IC application. To improve SOFC-IC performance of FSS, wide-varieties of protective/functional surface modifications and coatings have been investigated [4–12]. The functional requirements for protective coatings on FSS for SOFC-IC application are multifold, e.g., they must: 1) serve as a barrier against inward transport of oxidising species and outward transport of Cr-containing species (both gas and solid phases); 2) retain low ASR (<100 mΩ cm^2); and, 3) exhibit thermal-mechanical and chemical compatibility with adjoining stack components, e.g., no deleterious reactions with electrode or seal materials. Combined satisfaction of the above requirements must be achieved to the extent that SOFC stack voltage degradation is insignificant, e.g., less than ~0.1%/1,000 h, throughout the desired SOFC system life-time. In addition, SOFC-IC materials must be amenable to high-throughput and low cost production to meet anticipated market demands, e.g., 700 MW $year^{-1}$ planar SOFC module production at ~70 W/SOFC would require the production of ~10,000,000 ICs per year. These requirements challenge global research and development efforts.

Beyond the practice of pre-oxidation to form a dense, adherent Cr_2O_3 scale [13], the most well-known solutions are: coatings with Reactive Elements (normally Rare Earths) using sol-gel methods, chemical and physical vapour deposition (CVD and PVD) methods [14]; R.E. oxides deposition by PVD followed by a conditioning thermal treatment [15]; perovskite coatings by thermal spray [16], or other wet processes, eliminating the conditioning step at high temperature. Surface modifications and coatings on FSS for the SOFC-IC application range in both composition and architecture. Examples of common SOFC-IC coatings include: 1) perovskites with similar composition to SOFC cathode and previous interconnect materials (e.g., $La_{1-x}Sr_xMnO_3$, doped-$LaCrO_3$); 2) spinels with different mixtures of cations [e.g., $(Co,Mn)_3O_4$ or $(Cu,Mn)_3O_4$]; and, 3) corundum-type oxides with different cation ratios [e.g., $(Cr,Al)_2O_3$]. These coatings vary in thickness from submicron to over 20 μm and are applied using different solution and vapour-based techniques. All these methods tend to improve the adherence of the scale, increase the electron conductivity (lower ASR), reduce or eliminate the ionic conductivity (oxidising species through the scale to the alloy) and reduce Cr(VI) volatile species transport into electrodes.

In this study, metal organic chemical vapour deposition (MO-CVD) and large area filtered arc deposition (LAFAD) were employed for investigating surface modifications and coatings for FSS SOFC-IC application.

2 Experimental

2.1 MO-CVD

At high temperature, the reactive elements which impart the greatest oxidation resistance to FSS are the elements from the lanthanide series and yttrium. This is why La_2O_3, Nd_2O_3 and Y_2O_3 were deposited on Crofer22APU (ThyssenKrupp VDM), AL453 (Alleghany Ludlum), and Fe30Cr

by MOCVD in order to form perovskite oxides such as $LaCrO_3$, $NdCrO_3$ and $YCrO_3$ at high temperature. Despite its CTE, which is higher than that of other components of the cell, Haynes 230 (Haynes international), was also tested for comparison and in anticipation of eventual changes of the electrode/electrolyte materials.

Prior to deposition, the samples of Crofer22APU, AL453 and Haynes230 were cut in squares 1 × 1 cm × ~2 mm thick, and the samples of Fe30Cr were cut in discs of 1 cm diameter × ~1 mm thick. The samples were polished from 240-grit silicon carbide up to 1 µm with diamond paste. They were finally cleaned in ethanol in an ultrasonic bath and dried.

Details of the MOCVD coating process parameters have been described elsewhere [17]. This technique forms thin nanostructured oxide films about 100–500 nm thick.

2.2 Oxidation tests and ASR measurements

Uncoated and coated samples were oxidised in 800 °C laboratory air at atmospheric pressure for 100 h. During these exposures, the samples were continuously weighed in a thermobalance in order to acquire oxidation kinetics. The parabolic rate law was verified by plotting $\Delta m/A$ versus $t^{1/2}$ [18], where Δm is the mass gain of the samples (g), A the total oxidised area of the sample (cm^2) and t is the oxidation time (s). The slopes were analysed to determine parabolic rate law constants, k_p ($g^2\ cm^{-4}s^{-1}$).

The electrical resistivity measurements of the oxidised alloy were performed on uncoated and coated samples. Details of the ASR measurements have been given elsewhere [19]. The area-specific resistance (ASR) parameter reflects the resistance, the thickness, as well as the electrical properties of the oxide layers. The resistivity of the alloy substrate is negligible compared to that of the thermally grown oxide layer. The ASR is given by the following equation [20]:

$$ASR = 2\frac{M_{Cr_2O_3} \times \sqrt{k_p \times t}}{\left(3 \times M_O \times \rho_{Cr_2O_3}\right) \times \sigma}$$

where σ is the total conductivity of the oxide layer in S cm^{-1}, k_p the parabolic rate law constant, $M_{Cr_2O_3}$ and M_O the molar mass of chromia and of oxygen, respectively, $\rho_{Cr_2O_3}$ the density of chromia and t the exposure time.

2.3 LAFAD

LAFAD coatings were deposited on sheets (100 × 100 × 1 mm) of FSS 430 (acquired from Allegheny Ludlum). Details of the LAFAD coating process parameters and basic coating characteristics are provided elsewhere [4]. For reference, a simplified schematic of the LAFAD system is shown in Fig. 1. Two metal alloy cathode arc targets oppose each other on a chamber wall-mounted dual large area filtered arc source.

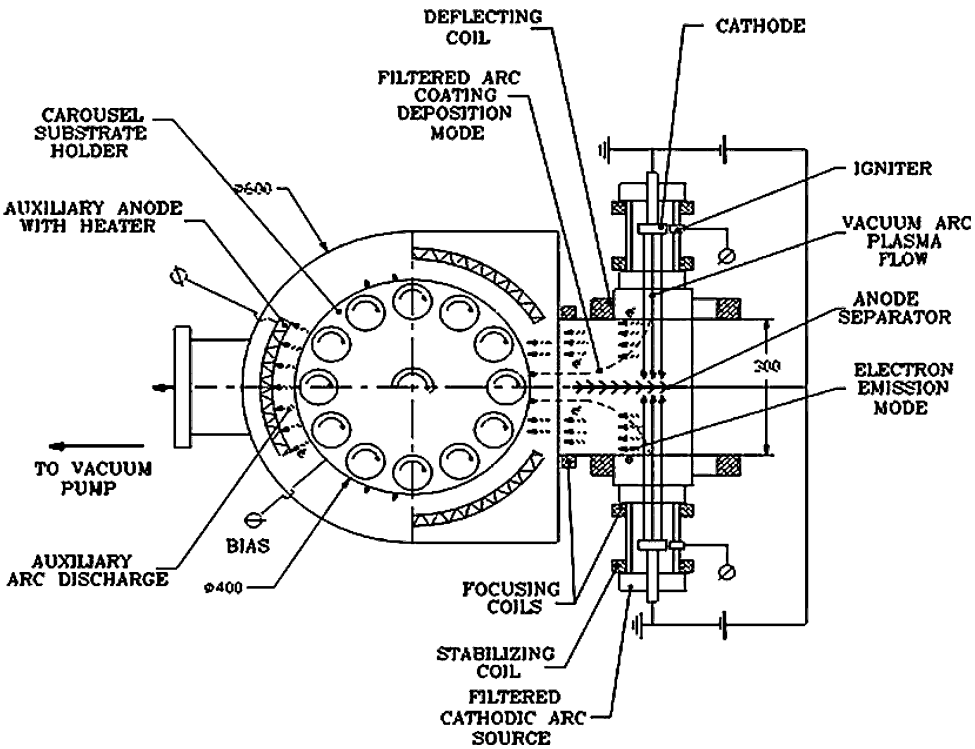

Fig. 1 Schematic plan-view of the LAFAD coating system

Prior to coating, specimen tabs of specific geometries for various SOFC-IC relevant exposure tests were cut with a N_2 laser (JE Soares, Inc.—Belgrade, MT, USA). Figure 2 presents photographs of typical coated and uncoated FSS 430 substrate sheets (100 × 100 × 1 mm) showing laser cut specimens attached via ~1 mm tabs. The optical interference observed on the coated sheet (right in Fig. 2) indicates vertical coating thickness variations from the middle (thickest) to the top and bottom margins. Vertical coating thickness variations result from disabling the scanning magnetic field coil within the LAFAD system and are used to investigate coating behaviour vs. thickness.

2.4 Coating properties characterisation

Coating thickness was determined using the CALOtest™ spherical abrasion technique and optimal microscopy with an accuracy of ±0.1 μm. Coating adhesion was assessed by means of the Mercedes indentation test using a Rockwell C indenter with ~100 N load [21]. Oxidation of the specimen tabs (in 800 °C air) was carried out using a standard furnace operated without control of humidity or air circulation (Bozeman, MT ambient). ASR measurements were made as a function of time in 800 °C air using two identical specimens faced opposite each other with porous $La_{0.8}Sr_{0.2}O_3$ (LSM) paste contacts in a standard 4-point probe geometry. Prior to ASR measurements, both uncoated and coated FSS 430 specimens were pre-oxidised in air at 800 °C for 100 h. Subsequent to varying exposure times, sample cross sections for microscopic analysis were prepared by epoxy-mounting, sectioning and polishing. Analytical techniques are described elsewhere [22].

3 Results and discussion

3.1 MOCVD results

The oxidation test of uncoated and coated alloy in air at 800 °C showed that the oxidation kinetics obeyed a parabolic rate law. The parabolic rate constant deduced from these experiments are indicated in Fig. 3. For uncoated materials, Haynes 230 alloy displays the best behaviour compared to ferritic alloys. For the uncoated Fe30Cr and AL453, the k_p values after 100 h at 800 °C in air are high; as a matter of fact, these alloys cannot be used as interconnects without a coating. In the case of ferritic alloys, the values of the parabolic rate law constants of the coated samples are lower than that of the uncoated specimens. It is interesting to note that, in contrast to AL453 alloy, in the case of Fe30Cr and Crofer22APU alloys, the coating effect does not depend on the nature of the reactive element; the k_p values are equally decreased. In the case of Haynes230, the effect of coating is not clearly visible; the values of the parabolic rate law constants of the uncoated and coated samples are close to each other.

The study of electrical properties (Fig. 4) of the oxide scales formed on uncoated Crofer22APU, AL453, Fe30Cr and Haynes230 showed that they were well adapted for use as interconnect. In fact, after 100 h at 800 °C the ASR parameter is lower than the limit of 0.1 Ω cm^2 generally reported in the literature [23]. After 40,000 h, an evaluation shows that this ASR parameter is equal to 0.9 Ω cm^2 for Crofer22APU, 1.0 Ω cm^2 for AL453, 0.6 Ω cm^2 for Fe30Cr and 1.1 Ω cm^2 for Haynes230; these values are higher than the limit of 0.1 Ω cm^2. ASR measurements of coated alloys showed that the presence of a reactive element oxide thin film also modified the electrical conductivity of the oxide scale. The evolution of electrical

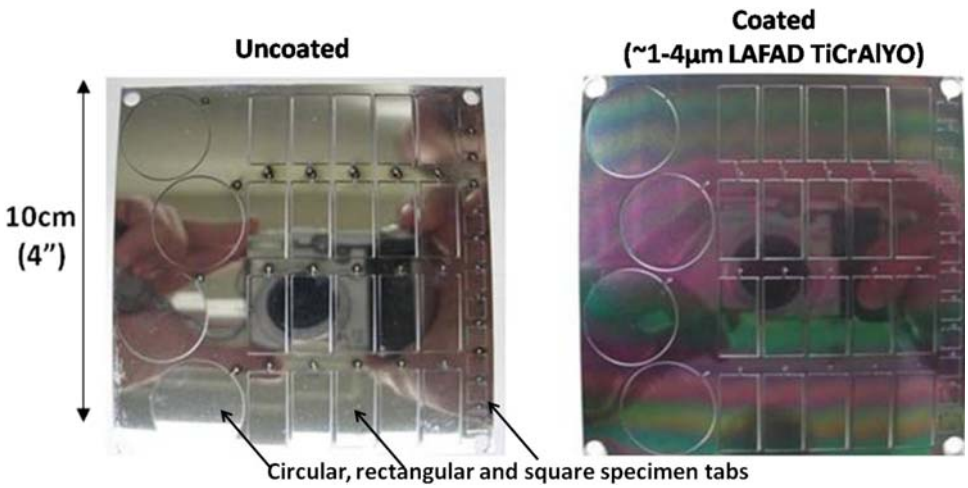

Fig. 2 Photographs of FSS sheet with and without LAFAD coating

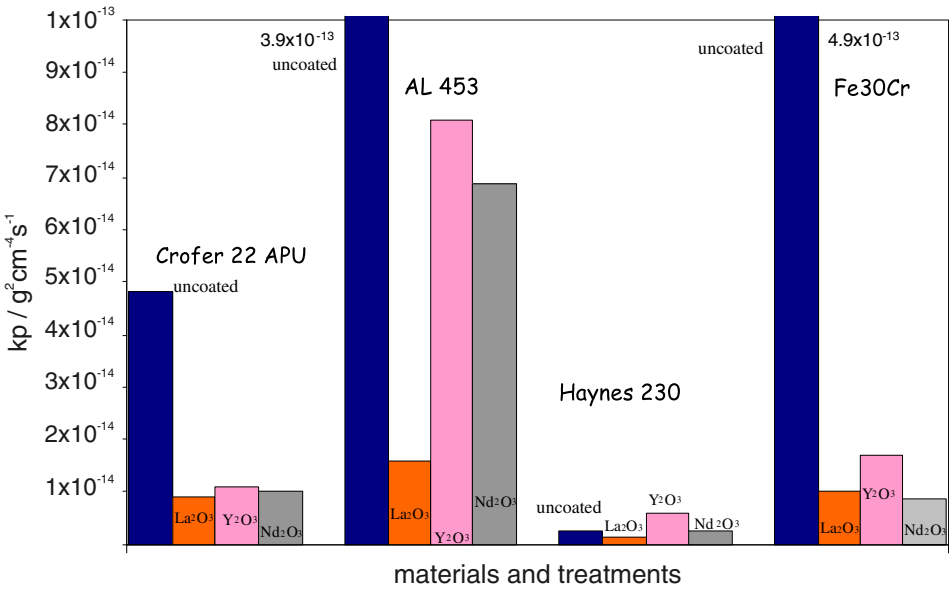

Fig. 3 Values of the parabolic rate constants kp for coated and uncoated samples of Crofer22APU, AL453, Haynes230 and Fe30Cr after 100 h at 800 °C in air under atmospheric pressure

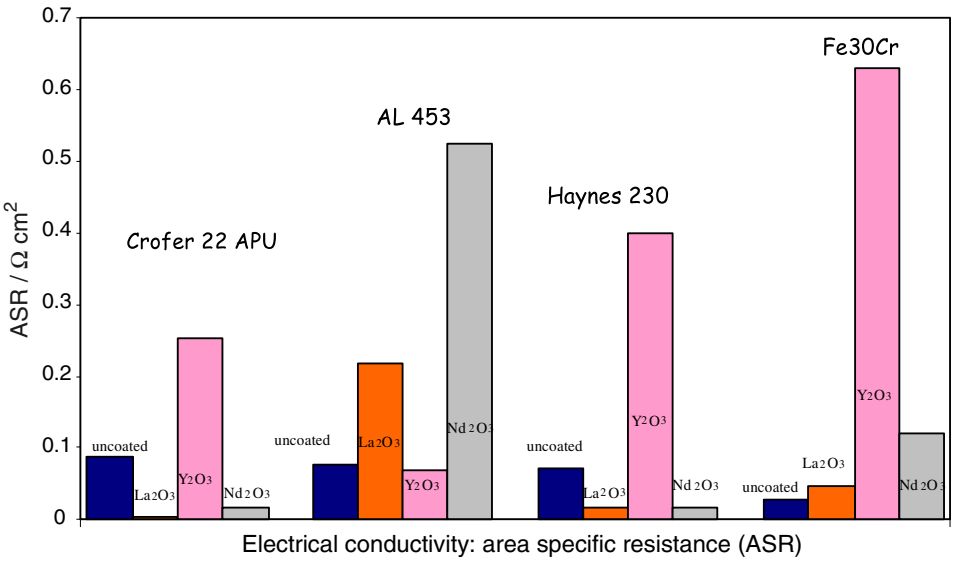

Fig. 4 Values of ASR parameter for coated and uncoated samples of Crofer22APU, AL453, Haynes230 and Fe30Cr after 100 h at 800 °C in air under atmospheric pressure

properties of coated alloys depends on the reactive element and the metallic substrate. As expected in the case of AL453, the yttrium oxide increased the electrical resistivity of the scale compared to the uncoated alloy. After 100 h, the ASR parameter is higher than the authorised limit. This phenomenon can be explained by the fact that, after 100 h at 800 °C, yttria is still present, not yet reacted with chromia to form a perovskite phase, and the electrical conductivity of yttria is lower than that of chromia. It is clear that the La_2O_3 coating improves the electrical conductivity of the oxide scale, particularly in the case of La_2O_3-coated Crofer22APU the ASR parameter is only 0.004 Ω cm^2. Moreover, after 40,000 h this parameter is 0.035 Ω cm^2. The presence of $LaCrO_3$, which has good electrical conductivity after 100 h at 800 °C, explains the decrease in the ASR. Moreover, SIMS (Secondary Ion Mass Spectrometry) experiments showed that the perovskite phase is probably doped by iron ions which considerably improve the perovskite phase conductivity.

3.2 LAFAD results

The most-promising SOFC-IC coating results to-date from LAFAD technology are realised with oxide coatings containing combinations of diffusion barrier components (e.g., Al_2O_3) and conductive components (e.g., Mn-containing oxides). Coatings have demonstrated excellent thermal stability, low and stable ASR (<25 mΩ cm^2 for >1,500 h) and negligible Cr volatility at 800 °C [22]. Figure 5 presents SEM surface (top) and cross section (bottom) images

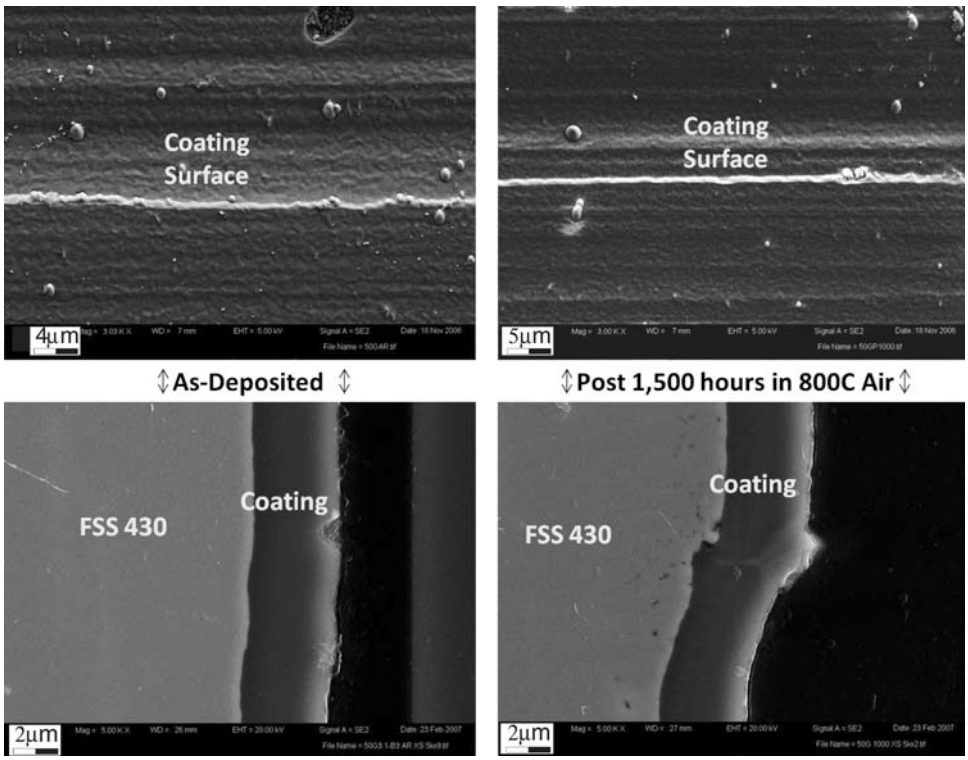

Fig. 5 Surface and cross section SEM images of LAFAD AlCrTiYO coating before and after 1,500 h in 800 °C air

of amorphous LAFAD AlCrTiYO coatings before (left) and after (right) >1,500 h in 800 °C air. This coating retained its thickness, with localised regions exhibiting outward Mn transport from the steel, which effects a decrease in ASR over time [22].

4 Conclusion

FSS are promising candidates for SOFC-IC materials operating at temperatures less than 800 °C. Protective and functional surface modifications and/or coatings can significantly improve FSS SOFC-IC performance and durability. Both MOCVD and LAFAD technologies have been successfully demonstrated for this application.

Proton-conducting SOFCs may introduce additional challenges for FSS interconnects. Since steam is produced at the cathode side, the additional moisture may affect air-side corrosion behaviour. Furthermore, hydrogen transport through FSS may be affected by the absence of water vapour in the anode gas phase, as is the case for oxygen ion conducting SOFCs. It has been reported that the TGO layer formed on FSS 430 in moist-hydrogen slows hydrogen transport through the bulk (from the fuel/anode-side), thereby reducing the anomalous effects of dual atmosphere air-side corrosion.

Future research should focus on characterising fundamental corrosion/protection processes for coated and uncoated FSS in conditions relevant to proton-conducting SOFCs. In addition, attention should be directed toward the technical and economical aspects involved with industrial scale-up of coating technologies.

References

1. Minh NQ (1993) J Am Ceram Soc 76:563
2. Singhal SC, Kendall K (2004) High temperature solid oxide fuel cells: fundamentals designs and applications. Elsevier Science, Oxford
3. Cable TL, Sofie SW (2007) J Power Sources 174:221
4. Gannon PE, Gorokhovsky VI, Deibert MC et al (2007) Int J Hydrogen Energy 32:3672
5. Elangovan S, Balagopal S, Timper M et al (2004) J Mat Eng Performance 13:265
6. Paldey S, Deevi SC (2003) Mat Sci Eng A342:58
7. Larring Y, Norby T (2000) J Electrochem Soc 147:3251
8. Yang Z, Xia G, Stevenson JW (2005) Electrochem Solid State Lett 8:A168
9. Chen X, Hou PY, Jacobson CP et al (2005) Solid State Ionics 176:425
10. Stanislowski M, Froitzheim J, Niewolak L et al (2007) J Power Sources 164:578
11. Gorokhovsky VI, Gannon PE, Deibert MC et al (2006) J Electrochem Soc 153:A1886
12. Fu CJ, Sun KN, Zhang NQ et al (2008) Thin Solid Films 516:1857
13. Capitianm MJ, Paul A, Pastol JL et al (1999) Oxid Met 52:447
14. Qu W, Li J, Pouglas GI (2004) J Power Sources 138:162
15. Zhu JH, Zhang Y, Basu A et al (2004) Surf Coat Technol 65:177
16. Schiller G, Henne R, Ruckdäschel R (2000) J Adv Mater 32:3
17. Chevalier S, Bonnet G, Larpin JP (2000) App Surf Sci 167:125
18. Pierragi B (1987) Ox Met 27:177

19. Fontana S, Amendola R, Chevalier S et al (2007) J Power Sources 171:177
20. Huang K, Hou PY, Goodenough JB (2000) Solid State Ionics 129:237
21. Jehn H, Reiners G, Siegel N (1993) DIN-Fachbericht 39. Beuth-Verlag, Berlin
22. Gannon P, Deibert M, White P et al (2008) Int J Hydrogen Energy 33:3991
23. Zhu WZ, Deevi SC (2003) Mat Sci Eng A348:227